3D macro/mesoporous highly reproducible amino-functionalized nanospheres for fat-rich foodstuffs pretreatment in nontargeted analysis

Yan Qi, Jing Zhang, Li Zhang, Xiangyu Zhou, Wei Li, Yushen Jin, Junwang Tang, Jianzhong Shen and Bing Shao*,*

Y. Qi, B. Shao, J. Shen

College of Veterinary Medicine

China Agricultural University

Beijing 100193, China

E-mail: shaobingch@sina.com (B. S.)

J. Zhang, X. Zhou, Y. Jin, B. Shao

Beijing Key Laboratory of Diagnostic and Traceability Technologies for Food Poisoning

Beijing Center for Disease Prevention and Control

Beijing 100013, China

E-mail: jinyushen2010@126.com (Y. J.)

L. Zhang

College of Science

China Agricultural University

Beijing 100193, China

W. Li

College of Chemistry

Nankai University

Tianjin 300071, China

J. Tang

Department of Chemical Engineering,

University College London

Torrington Place, London 10 WC1E7JE, UK

Abstract

Moving from the targeted to nontargeted analysis of chemical hazards in foods is an extremely challenging task for human wellbeing since various types of endogenous and exogenous substances are kept unknown for analysts. Lipids with a wide size distribution are the dominant interference in fat-rich foodstuffs. At present it is difficult to remove all lipids with one material. Herein for the first time diverse lipids from both animal and vegetable oils have been effectively removed and more than 400 chemical hazards with various physicochemical properties have been recovered. Such unprecedented function is due to the rational designed CTAB/TFBD-NH_2 which are three-dimensional (3D) macro/mesoporous amine-functionalized nanospheres. In detail CTAB was used as a structure-directing agent to guide the preparation of macro channels to decrease mass transfer resistance. Amino groups and mesoporous that is the key for capturing lipids was introduced via a facile building block exchange (BBE) strategy. Fundamentally it has been found that the mechanisms to universally capture free fatty acids (FFAs) and triglycerides (TGs) are hydrogen bonding, size exclusion and size filling, H-π effect, respectively. This has been evidenced by theoretical calculations, isothermal titration calorimetry (ITC), UPC^2-Q-TOF/MS and UPC^2-MS/MS. Overall this work highlights the substantial application potential of macro/mesoporous imine-linked 3D nanospheres to universal analysis in food safety and integrity.

Keywords: Macro/mesoporous nanospheres, Nontargeted analysis, Fat-rich foodstuffs, Chemical hazards, Adsorption mechanism

1. Introduction

Food safety and integrity is a challenging analytical task since varieties of unknown exogenous substances may be adulterated into foods by various pathways.[1] At present, most analytical strategies in food safety and integrity events are targeted methods, which means that some intentional contaminants or adulterants not on a target list cannot be identified.[2, 3] Considering the unoptimistic situation of global food safety, complementary nontargeted screening is highly advisable and has turned into a new research focus.[4] In 2015, the FDA issued the research strategic plan, including the development of nontargeted screening analytical methods for new, emerging and unidentified chemicals of concern.[5] The Chinese government also laid down a strategic plan for food safety, emphasizing the establishment of a combined, nontargeted inspection and testing technology system.[6] Owing to the complexity of the food matrix and the diversity of chemical hazards, effective sample pretreatment for nontargeted analysis is essential.[7] In particular, plant phytochrome in vegetables and lipids in fat-rich foodstuffs may strongly interfere with analytes.[4, 8] Therefore, efficient removal of these endogenous interferences and the maintenance of recoveries for concerned chemical hazards are essential for limiting interference and improving sensitivity and reproducibility.[2]

In our previous study, we elaborately designed a hierarchically micro- and mesoporous metal organic framework (MOF) to remove the phytochromes in vegetables and fulfill the nontargeted analysis.[4] Routinely, liquid-liquid extraction, gel permeation chromatography, and disposable solid-phase extraction adsorbents such as primary secondary amine (PSA) are used for fat removal, which are time- and organic solvent-consuming and labor-intensive.[8-10] Most importantly, in fat-rich foodstuffs, lipophilic analytes are also lost because of nonspecific adsorption.[4, 9, 11] Currently, novel materials, such as covalent organic frameworks (COFs)[12] and MOFs[13], show promise for sample pretreatment of foodstuffs, despite only a few reports on the application of them in nontargeted screening.[14, 15] Unlike phytochromes in vegetables, there are many

kinds of lipids (including triglycerides (TGs) and free fatty acids (FFAs)) in fat-rich foodstuffs that have a wide size distribution due to different carbon chain lengths and saturation. It is difficult to develop a porous material covering all sizes of the lipids. Thus, developing new materials that can successfully remove diverse lipids while retaining chemical hazards with different physicochemical properties in fat-rich foodstuffs is very urgent.

COFs with permanent porosity, highly ordered structures and abundant active sites have attracted extensive attention.[16-19] 3D COFs have become promising candidates for excellent adsorbents owing to their synthetically controllable, functionally manageable, large surface areas and high density of open sites.[20, 21] The current method for designing 3D COFs needs to introduce at least one building unit with T_d or orthogonal geometry to guide the extension of the polymer backbone into a covalently linked 3D network.[22, 23] However, 3D COFs are not only difficult to predesign and synthetically control but also have much lower porosity than expected due to the multifold interpenetration occupying the space.[24] Therefore, designing 3D COFs with high porosity and decreased mass transfer resistance is challenging. Imine-linked COFs (ICOFs) are one of the most widely used kinds of COFs that form via the polymerization of aldehydes and amines.[25] By introducing various functional groups or side groups, the potential performance and applicability of COFs can be improved.[26] However, due to the participation of amino groups in the assemblage of ICOFs, preparing *de novo* amino-functionalized ICOFs (ICOFs-NH_2) is a great challenge.[27]

Therefore, the aim of the present study is to synthesize 3D macro/mesoporous COF nanospheres with functional groups to remove lipids (including TGs and FFAs) from fat-rich foodstuffs and achieve efficient recoveries of different chemical hazards. 3D ICOF (CTAB/TFPA) nanospheres were developed with the simply addition of hexadecyl trimethyl ammonium bromide (CTAB), and the amino groups were introduced *via* a facile building block exchange (BBE) strategy to obtain CTAB/TFBD-NH_2 (Figure 1A). The prepared CTAB/TFBD-NH_2 nanospheres presented a loose and porous sphere-like morphology and possessed macro/mesoporous channels that dramatically increased the specific surface. The mesopores of the as-prepared materials

matched the dimensions of the main TGs and facilitated the smooth entry of FFAs; the macropores were conducive to mass transfer and a decreased resistance. Hydrogen bonding and size exclusion were the adsorption mechanisms of FFAs, and the size filling effect and weak H-π effect were the adsorption mechanisms of TGs. The results demonstrated that our nanospheres worked well for the removal of lipids from both animal and vegetable oils and held excellent recoveries for more than 400 chemical hazards (Scheme S1).

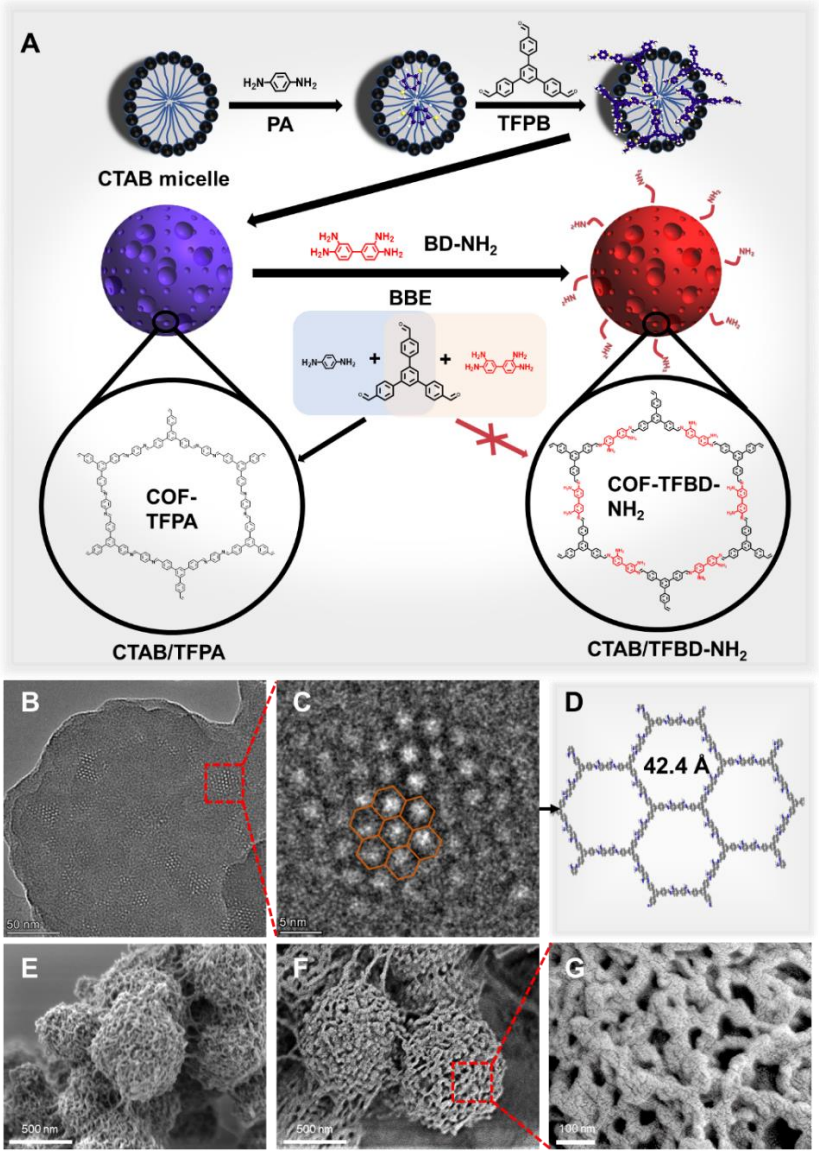

Figure 1. (A) Schematic depiction of the preparation of CTAB/TFBD-NH_2 nanospheres. (B) HRTEM image of TFBD-NH_2. (C) Enlarged view of a selected area in panel (B). (D) Crystal structures viewed through vertical projection of TFBD-NH_2 (gray, C; blue, N; white, H). (E) SEM image of CTAB/TFPA. (F) SEM image of

CTAB/ TFBD-NH_2. (G) Enlarged view of a selected area in panel (F).

2. Results and discussion

2.1 Preparation and characterization of CTAB/TFBD-NH_2

During the process of sample pretreatment, the obtained extracts extracted by acetonitrile typically contain a large amount of coextracted TGs and FFAs in fat-rich foodstuffs.[28] These matrixes can cause ion suppression or enhancement, which seriously interfere with the detection capability, repeatability and accuracy of the analysis method.[29] The sizes of TGs and FFAs are widely distributed due to their different carbon chain lengths and saturation. We chose lard and soybean oil as representative fat-rich foodstuffs to measure the amount of the TGs and FFAs (Figures S1 and S2). Three fatty acid methyl esters (FAMEs) with the highest content after methyl esterification were selected, and the sizes of TGs composed by them were calculated and listed in Table S1. The results showed that the largest sizes of TGs ranged from 34.1 Å to 41.7 Å. Therefore, two monomers, 1,3,5-tris(p-formylphenyl)benzene (TFPB) and diaminobenzidine (BD-NH_2), were selected to synthesize TFBD-NH_2 COFs. After geometric energy optimization of the TFBD-NH_2 COF structure under the P1M1 space group, its unit cell parameters were obtained (a=b=42.411 Å, c=3.515 Å) (Figures 1D and S3B), which matched the dimensions of the main TGs.

In this study, 2D ICOF TFPA was first synthesized by using TFPB and 1,4-phenylenediamine (PA) as monomers under the solvothermal preparation. Then, the *de novo* 2D amino-functionalized ICOF TFBD-NH_2 was prepared by displacing the PA in TFPA with BD-NH_2 *via* a facile building block exchange (BBE) strategy. 3D CTAB/TFBD-NH_2 nanospheres were prepared through introduction of CTAB in the synthesis process of 2D amino-functionalized ICOF TFBD-NH_2.

The morphological features of the materials were investigated by transmission electron microscopy (TEM), high-resolution transmission electron microscopy (HRTEM), and scanning electron microscopy (SEM). The prepared ICOFs TFPA and TFBD-NH_2 had 2D planar structures (Figures S4 and S5). After the BBE process, the morphology of both the 2D planar and 3D nanospheres were changed to different

degrees. The HRTEM image indicated that TFBD-NH_2 had an ordered alignment with a high degree of crystallinity (Figure 1B). Under high resolution, a honeycomb-like porous structure was visualized (Figure 1C) and the bright spots correspond to the pores (Figure 1D). The porous structure indicated a pore distance of about 4 nm in TFBD-NH_2, which is in excellent agreement with the simulated structure model (pore distance of 4.21 nm, Figure 1D). After the addition of CTAB, the CTAB/TFPA and CTAB/TFBD-NH_2 materials presented a loose and porous 3D sphere-like morphology with an average size of approximately 700 nm, which had macroporous channels visible to the naked eye (Figures 1E to 1G). As a kind of surfactant micelle, CTAB tends to form micelles with hydrophobic chains inside aqueous solution.[20] When PA monomer was added to the solution containing CTAB, the PA molecules assembled around the CTAB alkane chain due to the hydrophobicity. After the TFPB was added to the mixture, the TFPA polymer formed around CTAB immediately to formulate 3D nanospheres.

The crystallinity of the prepared material and the BBE process were verified by powder X-ray diffraction (PXRD). As shown in Figure 2A, the PXRD patterns of TFPA and CTAB/TFPA showed strong peaks at 2.98° and 2.90°, and relatively weak peaks at 5.22°, 7.72°, 10.22°, 12.78° and 5.12°, 7.56°, 10.10°, 12.66°, respectively, which coincided with the simulated pattern for TFPA produced with the space group *P1M1* (a = b =33.666 Å, c = 3.5222 Å) (Figures S7 and S3A). These results indicated the good crystallinity of the materials, and the introduction of the cationic micelle CTAB did not change their crystal structure. After the BBE process, the PXRD diffraction peaks of TFBD-NH_2 and CTAB/TFBD-NH_2 were observed at 2.46° and 2.54° (Figure 2B), which agreed well with the simulated structure of TFBD-NH_2 (Figures 2C).

The successful preparation of TFPA, CTAB/TFPA, TFBD-NH_2 and CTAB/TFBD-NH_2 was further confirmed by ^{13}C cross-polarization magic angle spinning solid-state nuclear magnetic resonance (CP-MAS SNMR) spectroscopy, Fourier transform infrared (FT-IR) spectroscopy and elemental analysis. As shown in Figure 2D, compared with TFPA, the ^{13}C NMR spectrum of TFBD-NH_2 after the BBE process showed great changes. In addition to the peak at 169.6 ppm, corresponding to the carbon of the amines, the ^{13}C NMR spectra of TFBD-NH_2 showed a new peak at 152.2 ppm

for the carbon of the aromatic amine, which was well matched with literature.[27] Additionally, the characteristic imine carbon signals all appeared at 157.2 ppm, 157.1 ppm, 158.1 ppm and 158.5 ppm for TFPA, CTAB/TFPA, TFBD-NH_2 and CTAB/TFBD-NH_2 (Figures 2E and F), respectively, proving the successful formation of the ICOFs.[30] The introduction of CTAB did not change the ^{13}C NMR spectra of materials. FT-IR spectroscopy was used to characterize the BBE process (Figure 2G). The typical imine stretching vibration band arising from C=N of all four materials at approximately 1610 cm^{-1} indicated the successful construction of ICOFs. After the BBE process, the new absorption bands observed at approximately 3190 cm^{-1} in TFBD-NH_2 and CTAB/TFBD-NH_2 were attributed to the stretching vibration of one N–H. Another N–H stretching at approximately 3445 cm^{-1} overlaid with the N–H stretching of incompletely reacted groups at the defects.[27] The elemental analysis showed that the contents of C (83.05%), H (4.79%), and N (7.95%) in TFPA were in good agreement with the analytically calculated contents of C (86.72%), H (4.85%) and N (8.43%). Also, the content of C (73.81%), H (4.67%), and N (12.11%) of TFBD-NH_2 was close to the analytically calculated content of C (82.16%), H (5.06%) and N (12.78%). However, the contents of C (82.37%), H (4.65%), N (7.68%) and C (74.22%), H (4.77%), and N (11.21%) of CTAB/TFPA and CTAB/TFBD-NH_2 changed to some degree compared with TFPA and TFBD-NH_2, which may be attributed to the remaining CTAB in the nanospheres. These results indicated the successful fabrication of the ICOFs and the success of the BBE process.

The surface areas and porosities of TFPA, CTAB/TFPA, TFBD-NH_2 and CTAB/TFBD-NH_2 were determined by nitrogen adsorption–desorption isotherms (Figures 2H and I). The Brunauer–Emmett-Teller (BET) surface areas of TFPA and TFBD-NH_2 were 56 m^2/g and 43 m^2/g, respectively. Nevertheless, the BET surface areas of CTAB/TFPA and CTAB/TFBD-NH_2 increased by approximately ten times to 563 m^2/g and 455 m^2/g, respectively, which could be attributed to the loose and porous structures in CTAB/TFPA and CTAB/TFBD-NH_2 (Figures 1E to G and Figures S5C, D). The larger surface area can provide many more reaction sites and active absorption sites.[31-33] Moreover, the average diameters of TFPA and TFBD-NH_2 were 32.6 Å and

41.5 Å, respectively. After the introduction of CTAB, the distribution of mesopore sizes for CTAB/TFBD-NH_2 ranged from 34.9 Å to 46.1 Å, which matched the dimensions of the main TGs (Table S1). In addition, CTAB/TFBD-NH_2 exhibited extra pores larger than 5 nm, leading to the full exposure of the interior mesopores and a dramatic improvement in the mass transfer rate.[14]

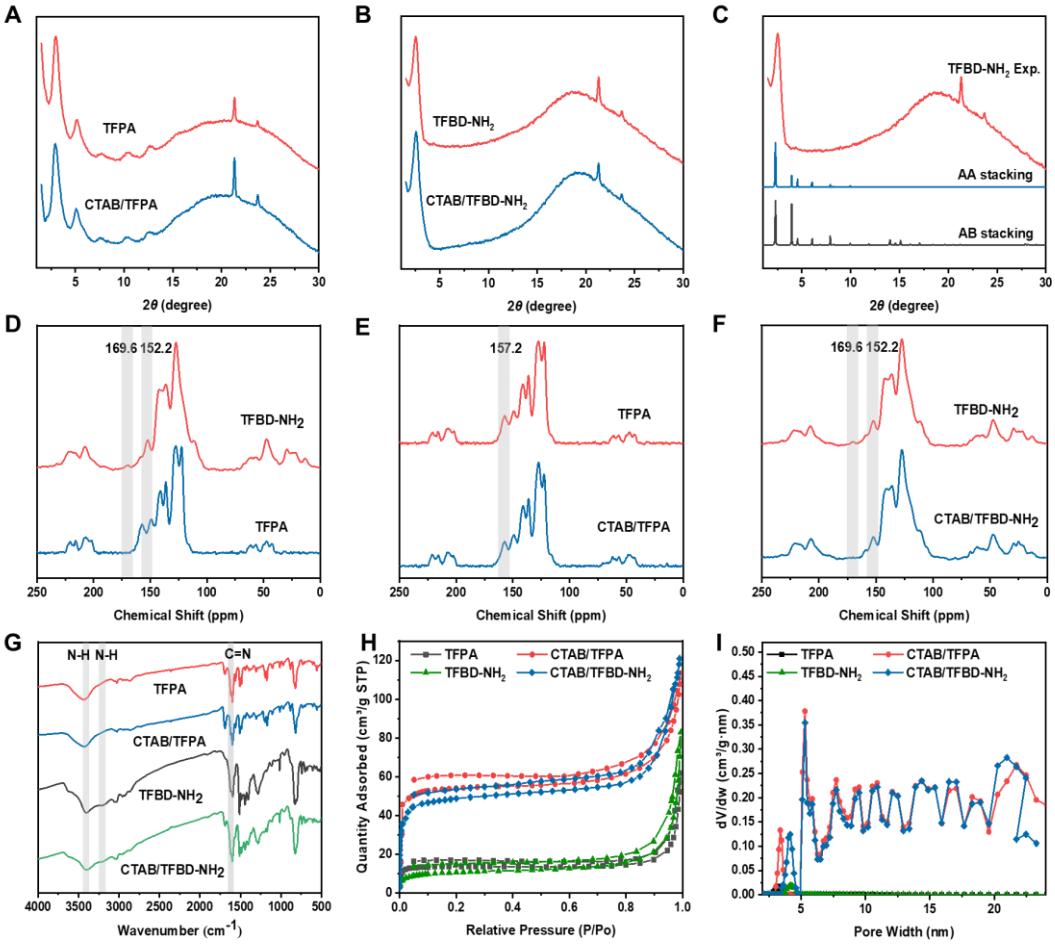

Figure 2. Characterizations of COFs. (A and B) PXRD patterns of TFPA, CTAB/TFPA, TFBD-NH_2 and CTAB/TFBD-NH_2 before and after BBE. (C) Experimental and simulated patterns (AA eclipsed model and AB staggered model) of TFBD-NH_2. (D to E) ^{13}C CP-MAS SNMR spectra, (G) FT-IR spectra, (H) N_2 adsorption–desorption isotherms and (I) pore size distributions of TFPA, CTAB/TFPA, TFBD-NH_2 and CTAB/TFBD-NH_2 before and after BBE.

2.2 Optimization of adsorption and desorption processes

To achieve the optimal adsorption and desorption performance for the removal of

lipids from animal and vegetable oils, the main parameters including the amounts of the sorbents, adsorption time, desorption solvent and reusability of the sorbents, were evaluated and optimized.

The optimal adsorbent dosage was evaluated by adding different amounts of CTAB/TFBD-NH_2 absorbent into 1 mL of acetonitrile extract from lard and soybean oil samples. As illustrated in Figure 3A, the removal efficiency of lipids increased rapidly with the adsorbent dosage from 5 to 20 $mg \cdot mL^{-1}$ and nearly reached a plateau above 20 $mg \cdot mL^{-1}$ in both lard and soybean oil samples. When the concentration of the adsorbents was 20 $mg \cdot mL^{-1}$, the removal efficiencies of lipids in lard and soybean oil were 87.5% and 89.6%, respectively. 20 mg CTAB/TFBD-NH_2 was selected for further experiments.

Adsorption is a time-dependent process. Thus, the adsorption equilibrium time was optimized. As shown in Figure 3B, whether for the lard samples or the soybean oil samples, the removal efficiency of lipids exhibited no obvious variation as the adsorption time increased from 10 seconds to 5 minutes. As the pretreatment time cannot be further reduced, 10 seconds was selected in subsequent experiments, which was much shorter than that used in the reported QuEChERS method and other sample pretreatment methods.[4, 34] Under the optimal adsorption processes, the CTAB/TFBD-NH_2 nanospheres exhibited excellent lipids removal efficiency both in lard (Figure 3E) and soybean oil (Figure 3F) samples.

Excellent reusability is one of the most important factors of adsorbents. To investigate the reusability of CTAB/TFBD-NH_2, the elution abilities of several organic solvents, including acetonitrile, hexane, methanol, ethanol, and acetone, were tested and compared (Figure 3C). Ethanol and acetone had satisfactory desorption efficiencies in both animal oil and vegetable oil. Considering that acetone was the final cleaning solvent for the CTAB/TFBD-NH_2 nanospheres synthesis process, acetone was selected as the elution solvent. To further evaluate the repetitive uses of CTAB/TFBD-NH_2, adsorption/desorption cycling experiments were conducted. After five cycles, the adsorption efficiency of CTAB/TFBD-NH_2 showed only a slight decrease, proving the excellent reusability of CTAB/TFBD-NH_2 nanospheres (Figure 3D).

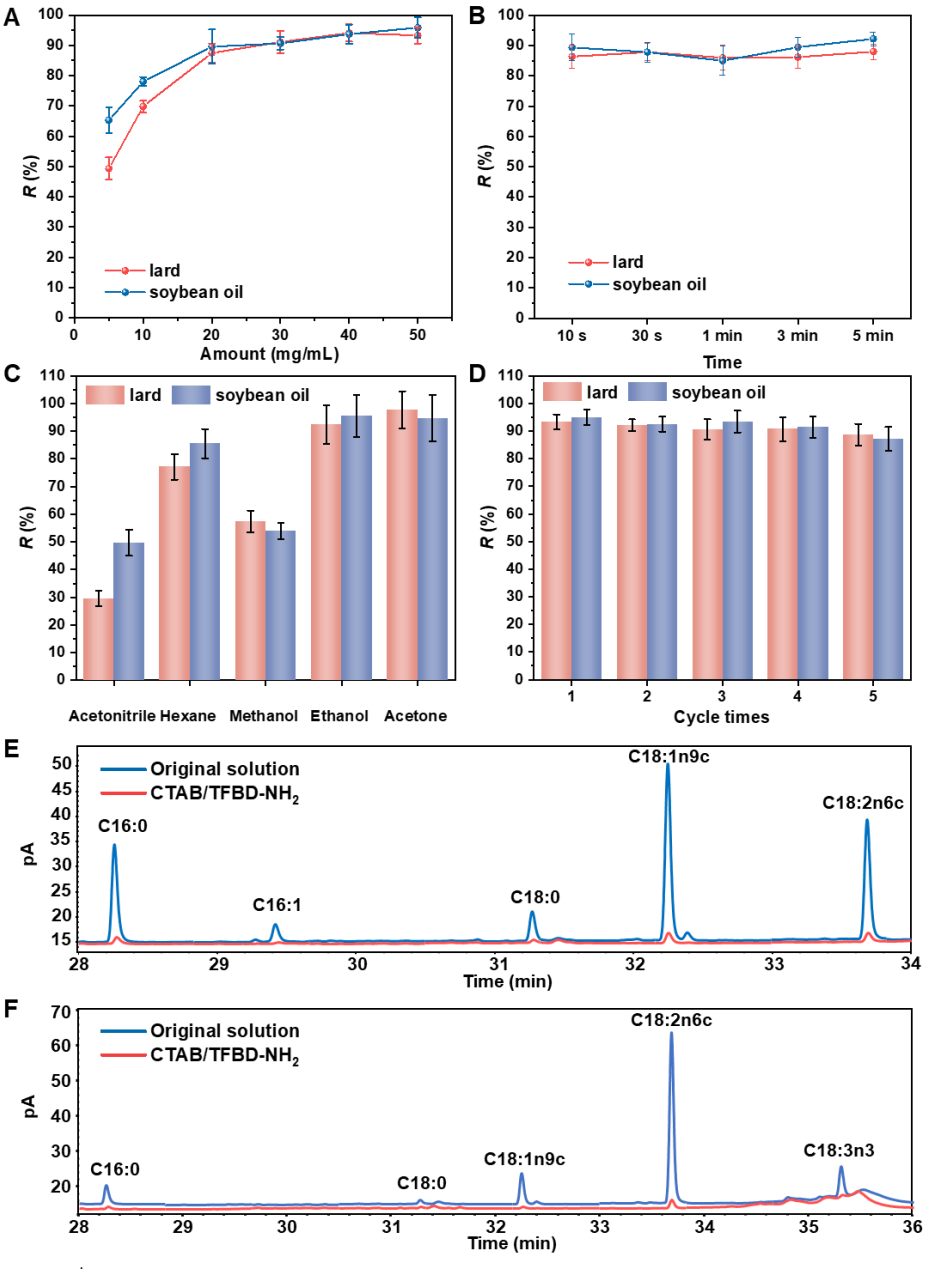

Figure 3. Optimization of lipid removal conditions and elution of lipids from CTAB/TFBD-NH_2. (A) Removal percentage of lipids after treatment with different amounts of CTAB/TFBD-NH_2. (B) Removal percentage of lipids after the addition of 20 mg mL^{-1} CTAB/TFBD-NH_2 with different adsorption times. (C) Elution efficiency of different eluents. (D) Five consecutive lipid adsorption/desorption cycles of CTAB/TFBD-NH_2. (E) The excerpt GC chromatograms (28-34 min) of FAMEs before and after lard adsorption procedures. (F) The excerpt GC chromatograms (28-36 min) of FAMEs before and after soybean oil adsorption procedures.

2.3 Feasibility of nontargeted analysis application

Sample pretreatment is a key step for the nontargeted detection of chemical hazards.[7] In nontargeted analysis, sample pretreatment should not only be highly selective in reducing complex matrix effects (MEs), but also be required to guarantee highly efficient recovery of a wide variety of analytes with various concentrations in different food samples.[2] Therefore, reducing MEs should be an important indicator for nontargeted analysis. A total of 276 pesticides (No. 1 to No. 276) and 131 veterinary drugs (No. 277 to No. 407) with different physicochemical properties (mass, chemical structures, polarities, acidity and alkalinity) (log Kow: -2.12-8.53 and pKa: -6.61-15.52) were selected as the chemical hazards to evaluate the feasibility of CTAB/TFBD-NH_2 for nontargeted analysis application in pork and soybean oil (Table S6 and Figure 4A). As listed in Table S7, among the 276 pesticides, ME values of 224 (81.2%) in pork and 221 (76.4%) in soybean oil were in the range of 0.7-1.3, indicating a mild matrix suppression or enhancement effect. At the same time, 44 (15.9%) in pork and 8 (2.9%) in soybean oil exhibited matrix enhancement effects, and 20 (7.2%) in pork and 45 (16.3%) in soybean oil displayed matrix suppression effects. For the 131 veterinary drugs, 79 (60.3%) in pork and 94 (71.8%) in soybean oil exhibited mild matrix suppression and enhancement effects. In addition, 42 (32.1%) in pork and 15 (11.5%) in soybean oil showed matrix enhancement effects, and 10 (7.6%) in pork and 22 (16.8%) in soybean oil exhibited matrix suppression effects. These results indicated that CTAB/TFBD-NH_2 can significantly remove MEs in the fat-rich animal and vegetable samples.

The recoveries of all the chemical hazards were calibrated with matrix-matched standards. As presented in Table S7 and Figure 4B, for pork samples, satisfactory recoveries (≥50%) were achieved for 275 (99.6%), 274 (99.3%), 273 (98.9%) pesticides and 122 (93.1%), 123 (93.9%), 123 (93.9%) veterinary drugs at all concentration levels (10, 50, and 100 μg kg^{-1}). The relative standard deviations (RSDs) ranged from 0.18-25.73%. For vegetable oil samples, satisfactory recoveries (≥50%) were achieved for all of the pesticides and 126 (96.2%), 129 (98.5%), 129 (98.5%) veterinary drugs at concentration levels of 10, 50, and 100 μg kg^{-1}, respectively. The RSDs ranged from

0.52-20.24%. Even several chemical hazards with low recoveries (20%-50%), all of them can be detected by instruments, indicating that our materials meet the requirements of nontargeted screening.

These results proved that the prepared CTAB/TFBD-NH_2 nanospheres as a kind of pretreatment material had immense potential for nontargeted analysis of chemical hazards with different physicochemical properties in different fat-rich foodstuffs.

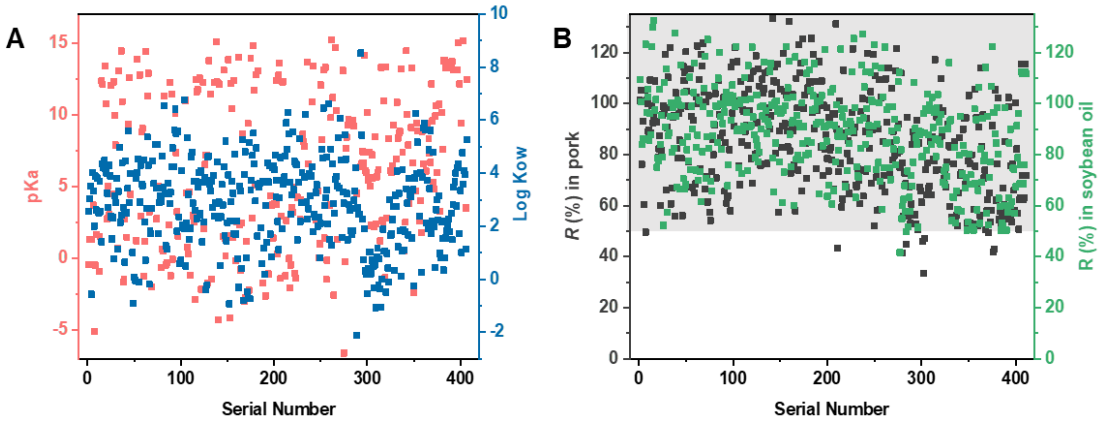

Figure 4. (A) Distribution diagram of dissociation constant (pKa) and n-octanol-water partition coefficient (log Kow) of 407 chemical hazards; (B). Average recovery ratio (*R*, %) at 50 μg kg^{-1} for pork and soybean oil of 407 chemical hazards.

2.4 Adsorption mechanism of CTAB/TFBD-NH_2 nanospheres

Considering the aromatic and amino ligand structures of CTAB/TFBD-NH_2 nanospheres, not only TGs and FFAs but also some chemical hazards may be adsorbed by CTAB/TFBD-NH_2 nanospheres via π-π interactions, hydrogen bonds and ion exchange. To further investigate the adsorption mechanism, lard was selected as the representative fat-rich foodstuff. High contents of FFA-C18:2n6c and TG-1-palmitin-2-olein-3-linolein in animal foods were chosen for the following experiments. The possible interaction mechanism was predicted by molecular docking, and the interaction energies were calculated by applying the density functional theory (DFT). BVTD (4,4'-bis(((E)-(4"-vinyl-[1,1':3',1"-terphenyl]-4-yl)methylene)amino)-[1,1'-biphenyl]-3,3'-diamine) (Figure S16) as the assembly building blocks of CTAB/TFBD-NH_2, was selected as the model compound. From the results of molecular docking, the

adsorption of C18:2n6c by BVTD was mainly through hydrogen bonding interactions. The main interaction between BVTD and 1-palmitin-2-olein-3-linolein was the H-π interaction between the benzene ring with amino substitution and the TG molecule (Figure S17). The DFT results revealed that the highest occupied molecular orbital (HOMO) of BVTD amino was consistent with the lowest unoccupied molecular orbital (LUMO) of C18:2n6c with respect to the symmetry of the wave function, indicating that they may interact through amino groups of BVTD and carbonyl groups of C18:2n6c (Figure 5A). For 1-palmitin-2-olein-3-linolein, LUMO was localized on the ester bond 1 (Figure 5B), which resulted in a weak H-π interaction on the methylene linked to ester bond 2. The interaction energy between BVTD and C18:2n6c was -15.75 kJ mol^{-1} (hydrogen bond), and that of 1-palmitin-2-olein-3-linolein was -0.04 kJ mol^{-1} (H-π interaction). The adsorption sites of BVTD were mainly concentrated on the amino and benzene rings with amino modification. BVTD adsorbed FFAs by forming hydrogen bonds and adsorbed TGs by forming H-π bonds. Moreover, the hydrogen bonding interactions between FFAs and BVTD were more stable than the H-π interactions.

To investigate the affinity of binding interactions, isothermal titration calorimetry (ITC) was used to explore the enthalpic and entropic changes arising from the interactions between CTAB/TFBD-NH_2 and the lipids (including FFA-C18:2n6c and TG-1-palmitin-2-olein-3-linolein). To mimic the previous adsorption process, the titration processes were carried out in acetonitrile. ITC thermograms for injections of acetonitrile into acetonitrile, acetonitrile into CTAB/TFBD-NH_2, C18:2n6c into acetonitrile and 1-palmitin-2-olein-3-linolein into acetonitrile were first examined to subtract the influence of the enthalpy of interactions between the analytes or CTAB/TFBD-NH_2 and acetonitrile. The observed peaks suggested that each injection exhibited a different degree of endothermic process (Figures S18 to S20 and Figures S22 to S23). Thermograms resulting from the titration of the suspension of CTAB/TFBD-NH_2 with the C18:2n6c and 1-palmitin-2-olein-3-linolein solutions displayed strong, negative peaks, meaning that C18:2n6c and 1-palmitin-2-olein-3-linolein adsorption proceeded via an exothermic pathway (Figures S19 and S22). After

the absorbed heat caused by the solvent enthalpy subtraction, the parameter space of C18:2n6c and 1-palmitin-2-olein-3-linolein adsorption in CTAB/TFBD-NH_2 is shown in Figure 5C and Table S8. For the titration of C18:2n6c into CTAB/TFBD-NH_2, the negative enthalpic term suggested the presence of hydrogen bonds,[17, 35] which was due to the presence of the amino group. The positive entropic term (ΔS) also suggested that the environment immediately surrounding the binding site became more disordered after adsorption of C18:2n6c. Combined with the binding constant n=1.514, we speculated that the mesoporous of CTAB/TFBD-NH_2 avoided the aggregation of C18:2n6c, and made them rotate freely in the mesoporous, which was conductive to the hydrogen bonds formation between the amino groups of CTAB/TFBD-NH_2 and carbonyl groups of C18:2n6c[17]. Furthermore, the negative Gibbs free energy change (ΔG=−17.12 kJ mol^{-1}) was close to the interaction energy predicted by DFT (-15.75 kJ mol^{-1}). The theoretical calculations and experimental results showed that hydrogen bonding and size exclusion are the main adsorption mechanisms of FFAs. For the titration of 1-palmitin-2-olein-3-linolein into CTAB/TFBD-NH_2, the thermodynamic data showed that both enthalpy change and entropy change were negative. The measured enthalpy reported the changes in noncovalent bond energies during the interaction.[35] The negative entropy rendered this adsorption entropically unfavorable. Since n=0.952, we speculated that the mesoporous size of CTAB/TFBD-NH_2 was similar to that of 1-palmitin-2-olein-3-linolein, rendering the molecules stuck in the mesopores and restricting their free movement. The negative Gibbs free energy change (ΔG=−19.97 kJ mol^{-1}) indicated that the adsorption process was favorable and spontaneous. However, it was quite different from the calculation results of DFT (ΔG=−0.04 kJ mol^{-1}), which may be attributed to the truncated component used in theoretical calculations, not the real structure of the CTAB/TFBD-NH_2, resulting in the ignored porous filling effect.

To further confirm our conjecture, PSA, containing primary and secondary amines, and TFBD-NH_2, prepared with a similar procedure without CTAB, were used as controls. Under the same adsorption procedures, nonporous PSA exhibited 5.31% removal efficiency of lipids (Figure 5E), indicating that almost no adsorption occurred

when only amino groups were present. And single mesoporous TFBD-NH_2 possessed 46.28% removal efficiency of lipids (Figure 5E), which might be due to the fact that the missing macroporous increased the mass transfer resistance. These results offered evidence that both macropores and mesopores were important for lipids adsorption, which could be used as a supplement to theoretical calculations and ITC results.

To more thoroughly understand the TGs and FFAs adsorption mechanism of CTAB/TFBD-NH_2 nanospheres, UPC^2-Q-TOF/MS and UPC^2-MS/MS were used for the determination of TGs and FFAs, respectively, before and after material adsorption. The ions extracted from UPC^2-Q-TOF/MS chromatograms (Figure S25) were consistent with the identification and quantification of TAGs reported in the literature.[36] CTAB/TFBD, which had a structure similar to that of CTAB/TFBD-NH_2 but no free amino groups, was employed as a control. As shown in Figure 5D and Table S9, the CTAB/TFBD-NH_2 nanospheres attained excellent TGs and FFAs removal efficiency, while CTAB/TFBD exhibited a poor removal efficiency. The reduction of removal efficiency may be due to the absence of amino groups (for FFAs) and the size distribution of the mesoporous (38.6-50.9 Å, Figure S14) not well matched with the dimensions of the main TGs (Table S1). Interestingly, the CTAB/TFBD-NH_2 nanospheres exhibited higher removal efficiencies for FFAs with longer carbon chains (Table S9). Combined with the ITC results, we speculated that the mesoporous of CTAB/TFBD-NH_2 avoided the aggregation of FFAs with long carbon chains, making them rotate freely in the mesoporous and the formation hydrogen bonds. However, when carbon chains of FFAs was shorter, more FFA molecules can enter the mesopores, which may result in the aggregation of the FFA molecules, limit the free rotation of the molecules and reduce the formation probability of hydrogen bonds.

Based on the above results, we boldly made the following mechanism speculation: (1) the adsorption mechanism of FFAs by CTAB/TFBD-NH_2 is mainly based on hydrogen bonding and size exclusion; and (2) the adsorption mechanism of TGs is mainly due to the size filling effect and is supplemented by the H-π effect. Therefore, some chemical hazards with dimensions similar to the pore size of the CTAB/TFBD-NH_2 nanospheres and/or strong hydrogen bonding interactions with amino groups on

the CTAB/TFBD-NH_2 nanospheres may also be adsorbed by the material.

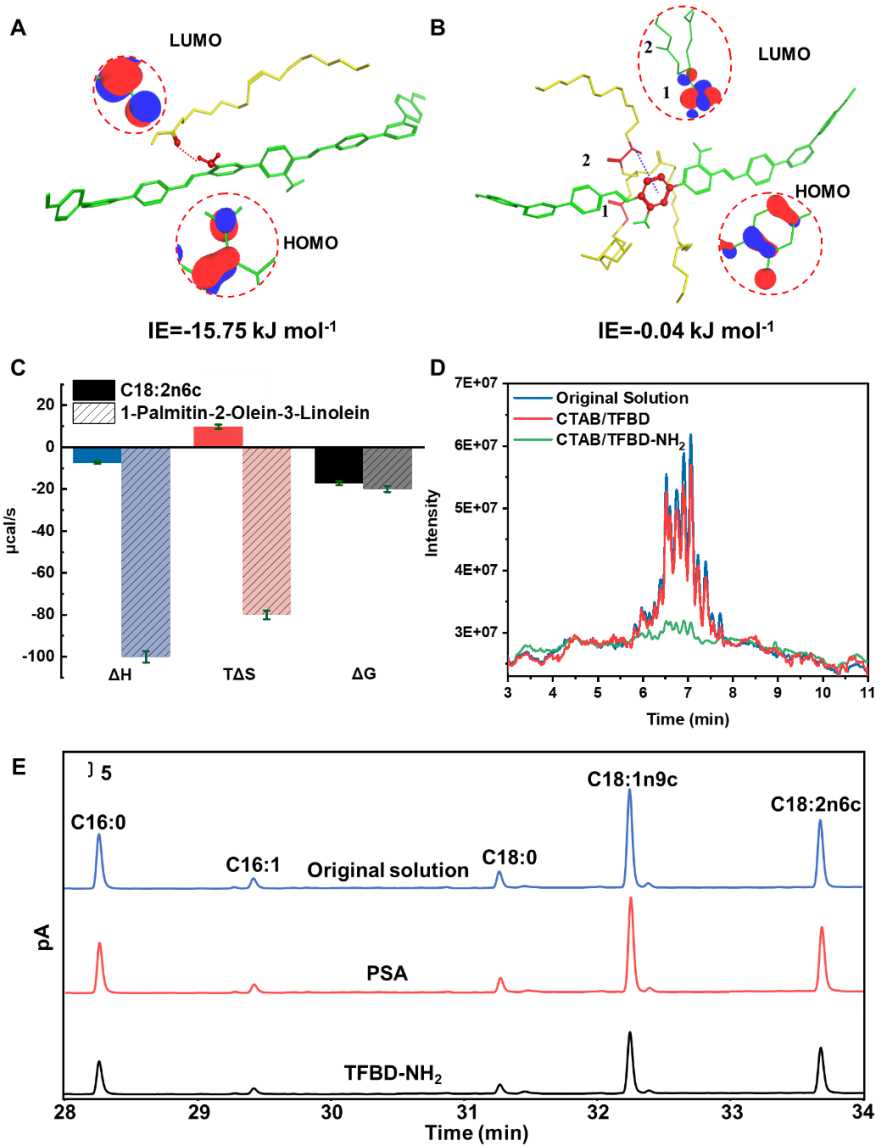

Figure 5. (A) Binding conformation and interaction energy (IE) of BVTD-C18:2n6c, HOMO of the amino group in BVTD and LUMO of the carbonyl group in C18:2n6c. (B) Binding conformation and interaction energy (IE) of BVTD-1-palmitin-2-olein-3-linolein, HOMO of the benzene ring with amino substitution in BVTD and LUMO of the methylene group linked with carbonyl group in 1-palmitin-2-olein-3-linolein. (Red-positive wave function, blue-negative wave function; red dotted line-hydrogen bonding interaction, blue dotted line-H-π interaction). (C) Thermodynamic parameters of C18:2n6c and 1-palmitin-2-olein-3-linolein in CTAB/TFBD-NH_2. (D) The excerpt UPC^2-Q-TOF/MS chromatograms (3-11 min) of TAGs after adsorption procedures. (E) The excerpt GC chromatograms (28-34 min) of FAMEs before and after lard

adsorption procedures.

3. Conclusion

In summary, for the first time, this study prepared 3D crystalline amino-functionalized macro/mesoporous COF nanospheres to remove lipids from fat-rich samples. The 3D CTAB/TFBD-NH_2 nanospheres were fabricated with CTAB as a structure-directing agent to form the macropore and 3D structures, and further through a building block exchange (BBE) strategy to introduce the functional amino groups. The prepared CTAB/TFBD-NH_2 had appropriate mesoporous pore sizes and functional groups for lipids removal, and the macroporous channels were conducive to the improvement of the mass transfer rate. Efficient recoveries for the more than 400 chemical hazards and excellent lipids removal capacity were achieved, indicating its great potential for nontargeted analysis in fat-rich foodstuffs. Molecular docking, DFT, ITC, UPC^2-Q-TOF/MS and UPC^2-MS/MS demonstrated that the hydrogen bonding and size exclusion were the main adsorption mechanisms of FFAs, and the porous filling effect and weak H-π effect were the main adsorption mechanisms of TGs. These results highlight the great potential of modification of crystalline porous materials, such as MOFs or other COFs, for the removal of specific interferences in complicated samples by controlling the pore sizes and anchoring functional groups on the crystalline porous materials.

Supporting Information

Supporting Information is available from the Wiley Online Library or from the author.

Acknowledgements

This work was supported by the National Key Research and Development Program of China (2018YFC1602400). The authors gratefully acknowledge Jianlong Yu at Waters Corporation with the assistance at UPC^2-MS/MS and UPC^2-Q-TOF/MS analysis.

References

1. Cavanna, D.; Righetti, L.; Elliott, C.; Suman, M., The scientific challenges in moving from targeted to non-targeted mass spectrometric methods for food fraud analysis: A proposed validation workflow to bring about a harmonized approach. *Trends in Food Science & Technology* **2018,** *80*, 223-241.

2. Shao, B.; Li, H.; Shen, J.; Wu, Y., Nontargeted Detection Methods for Food Safety and Integrity. *Annual Review of Food Science and Technology* **2019,** *10* (1).

3. Abbas, O.; Zadravec, M.; Baeten, V.; Mikus, T.; Lesic, T.; Vulic, A.; Prpic, J.; Jemersic, L.; Pleadin, J., Analytical methods used for the authentication of food of animal origin. *Food Chem* **2018,** *246*, 6-17.

4. Jin, Y.; Qi, Y.; Tang, C.; Shao, B., Hierarchical micro- and mesoporous metal–organic framework-based magnetic nanospheres for the nontargeted analysis of chemical hazards in vegetables. *Journal of Materials Chemistry A* **2021,** *9* (14), 9056-9065.

5. Center for Food Safety and Applied Nutrition Science and Research (CSR) Strategic Plan. https://www.fda.gov/Food/FoodScienceResearch/ResearchStrategicPlan/default.htm (accessed 2).

6. The 13th Five-Year Plan for National Food Safety. http://www.gov.cn/zhengce/content/2017-02/21/content_5169755.htm (accessed 2).

7. Li, W.; Jiang, H. X.; Geng, Y.; Wang, X. H.; Gao, R. Z.; Tang, A. N.; Kong, D. M., Facile Removal of Phytochromes and Efficient Recovery of Pesticides Using Heteropore Covalent Organic Framework-Based Magnetic Nanospheres and Electrospun Films. *ACS Appl Mater Interfaces* **2020,** *12* (18), 20922-20932.

8. Rejczak, T.; Tuzimski, T., QuEChERS-based extraction with dispersive solid phase extraction clean-up using PSA and ZrO2-based sorbents for determination of pesticides in bovine milk samples by HPLC-DAD. *Food Chemistry* **2017,** *217*, 225-233.

9. Jeong, I. S.; Kwak, B. M.; Ahn, J. H.; Jeong, S. H., Determination of pesticide residues in milk using a QuEChERS-based method developed by response surface methodology. *Food Chemistry* **2012,** *133* (2), 473-481.

10. Ly, T. K.; Ho, T. D.; Behra, P.; Nhu-Trang, T. T., Determination of 400 pesticide residues in green tea leaves by UPLC-MS/MS and GC-MS/MS combined with QuEChERS extraction and mixed-mode SPE clean-up method. *Food Chemistry* **2020,** *326* (1–2), 126928.

11. Feng, C.; Xu, Q.; Qiu, X.; Jin, Y.; Ji, J.; Lin, Y.; Le, S.; Wang, G.; Lu, D., Comprehensive strategy for analysis of pesticide multi-residues in food by GC-MS/MS and UPLC-Q-Orbitrap. *Food Chem* **2020,** *320*, 126576.

12. Romero, V.; Fernandes, S. P. S.; Rodriguez-Lorenzo, L.; Kolen'ko, Y. V.; Espina, B.; Salonen, L. M., Recyclable magnetic covalent organic framework for the extraction of marine biotoxins. *Nanoscale* **2019,** *11* (13), 6072-6079.

13. Li, B.; Dong, X.; Wang, H.; Ma, D.; Tan, K.; Jensen, S.; Deibert, B. J.; Butler, J.; Cure, J.; Shi, Z.; Thonhauser, T.; Chabal, Y. J.; Han, Y.; Li, J., Capture of organic iodides from nuclear waste by metal-organic framework-based molecular traps. *Nat Commun* **2017,** *8* (1), 485.

14. Li, W.; Gao, R.-Z.; Jiang, H.-X.; Lu, Q.-Y.; Tang, A.-N.; Kong, D.-M., Metal organic frameworks as sacrificial templates for preparation of hierarchical covalent organic frameworks enabling ultrafast sample treatment in nontargeted food safety analysis. *Chemical Engineering Journal* **2021,** *425*.

15. Li, W.; Wang, R.; Jiang, H. X.; Chen, Y.; Tang, A. N.; Kong, D. M., Controllable synthesis of uniform large-sized spherical covalent organic frameworks for facile sample pretreatment and as

naked-eye indicator. *Talanta* **2022,** *236*, 122829.
16. Grunenberg, L.; Savasci, G.; Terban, M. W.; Duppel, V.; Moudrakovski, I.; Etter, M.; Dinnebier, R. E.; Ochsenfeld, C.; Lotsch, B. V., Amine-Linked Covalent Organic Frameworks as a Platform for Postsynthetic Structure Interconversion and Pore-Wall Modification. *J Am Chem Soc* **2021,** *143* (9), 3430-3438.
17. Drout, R. J.; Kato, S.; Chen, H.; Son, F. A.; Otake, K. I.; Islamoglu, T.; Snurr, R. Q.; Farha, O. K., Isothermal Titration Calorimetry to Explore the Parameter Space of Organophosphorus Agrochemical Adsorption in MOFs. *J Am Chem Soc* **2020,** *142* (28), 12357-12366.
18. Yuan, C.; Wu, X.; Gao, R.; Han, X.; Liu, Y.; Long, Y.; Cui, Y., Nanochannels of Covalent Organic Frameworks for Chiral Selective Transmembrane Transport of Amino Acids. *J Am Chem Soc* **2019,** *141* (51), 20187-20197.
19. Tilford, R. W.; Mugavero, S. J., 3rd; Pellechia, P. J.; Lavigne, J. J., Tailoring microporosity in covalent organic frameworks. *Adv Mater* **2008,** *20* (14), 2741-6.
20. Zhang, S.; Wu, X.; Ma, C.; Li, Y.; You, J., Cationic Surfactant Modified 3D COF and Its Application in the Adsorption of UV Filters and Alkylphenols from Food Packaging Material Migrants. *J Agric Food Chem* **2020,** *68* (11), 3663-3669.
21. Han, X.; Huang, J.; Yuan, C.; Liu, Y.; Cui, Y., Chiral 3D Covalent Organic Frameworks for High Performance Liquid Chromatographic Enantioseparation. *J Am Chem Soc* **2018,** *140* (3), 892-895.
22. Chen, X.; Geng, K.; Liu, R.; Tan, K. T.; Gong, Y.; Li, Z.; Tao, S.; Jiang, Q.; Jiang, D., Covalent Organic Frameworks: Chemical Approaches to Designer Structures and Built-In Functions. *Angew Chem Int Ed Engl* **2020,** *59* (13), 5050-5091.
23. Lin, G.; Ding, H.; Chen, R.; Peng, Z.; Wang, B.; Wang, C., 3D Porphyrin-Based Covalent Organic Frameworks. *J Am Chem Soc* **2017,** *139* (25), 8705-8709.
24. Geng, K.; He, T.; Liu, R.; Dalapati, S.; Tan, K. T.; Li, Z.; Tao, S.; Gong, Y.; Jiang, Q.; Jiang, D., Covalent Organic Frameworks: Design, Synthesis, and Functions. *Chem Rev* **2020,** *120* (16), 8814-8933.
25. Segura, J. L.; Mancheno, M. J.; Zamora, F., Covalent organic frameworks based on Schiff-base chemistry: synthesis, properties and potential applications. *Chem Soc Rev* **2016,** *45* (20), 5635-5671.
26. Zhang, X.; Li, G.; Wu, D.; Zhang, B.; Hu, N.; Wang, H.; Liu, J.; Wu, Y., Recent advances in the construction of functionalized covalent organic frameworks and their applications to sensing. *Biosens Bioelectron* **2019,** *145*, 111699.
27. Qian, H.-L.; Li, Y.; Yan, X.-P., A building block exchange strategy for the rational fabrication of de novo unreachable amino-functionalized imine-linked covalent organic frameworks. *Journal of Materials Chemistry A* **2018,** *6* (36), 17307-17311.
28. Moreno-Gonzalez, D.; Alcantara-Duran, J.; Addona, S. M.; Beneito-Cambra, M., Multi-residue pesticide analysis in virgin olive oil by nanoflow liquid chromatography high resolution mass spectrometry. *J Chromatogr A* **2018,** *1562*, 27-35.
29. Mastrianni, K. R.; Metavarayuth, K.; Brewer, W. E.; Wang, Q., Analysis of 10 beta-agonists in pork meat using automated dispersive pipette extraction and LC-MS/MS. *J Chromatogr B Analyt Technol Biomed Life Sci* **2018,** *1084*, 64-68.
30. Peng, Y.; Wong, W. K.; Hu, Z.; Cheng, Y.; Yuan, D.; Khan, S. A.; Zhao, D., Room Temperature Batch and Continuous Flow Synthesis of Water-Stable Covalent Organic Frameworks (COFs). *Chemistry of Materials* **2016,** *28* (14), 5095-5101.
31. Xu, H.; Li, H.; Xie, L.; Zhao, D.; Kong, B., Interfacial Assembly of Functional Mesoporous

Carbon‐Based Materials into Films for Batteries and Electrocatalysis. *Advanced Materials Interfaces* **2022,** *9* (10).

32. Liang, J.; Zhou, R. F.; Chen, X. M.; Tang, Y. H.; Qiao, S. Z., Fe-N decorated hybrids of CNTs grown on hierarchically porous carbon for high-performance oxygen reduction. *Adv Mater* **2014,** *26* (35), 6074-9.

33. Liang, H. W.; Zhuang, X.; Bruller, S.; Feng, X.; Mullen, K., Hierarchically porous carbons with optimized nitrogen doping as highly active electrocatalysts for oxygen reduction. *Nat Commun* **2014,** *5*, 4973.

34. Concha-Meyer, A.; Grandon, S.; Sepulveda, G.; Diaz, R.; Yuri, J. A.; Torres, C., Pesticide residues quantification in frozen fruit and vegetables in Chilean domestic market using QuEChERS extraction with ultra-high-performance liquid chromatography electrospray ionization Orbitrap mass spectrometry. *Food Chem* **2019,** *295*, 64-71.

35. Chiad, K.; Stelzig, S. H.; Gropeanu, R.; Weil, T.; Klapper, M.; Müllen, K., Isothermal Titration Calorimetry: A Powerful Technique To Quantify Interactions in Polymer Hybrid Systems. *Macromolecules* **2009,** *42* (19), 7545-7552.

36. Yeo, J.; Parrish, C. C., Evaluation of triacylglycerol (TAG) profiles and their contents in salmon muscle tissue using ESI-MS/MS spectrometry with multiple neutral loss scans. *Food Chem* **2020,** *324*, 126816.